25

Controlled Fabrication of Noble Metal Nanomaterials via Nanosphere Lithography and Their Optical Properties

Yujun Song
Key Laboratory for Aerospace Materials and Performance (Ministry of Education), School of Materials Science and Engineering, Beihang University, Beijing, China

1. Introduction

Since ancient time, noble metal has been used to make ornaments, jewelry, high-value tableware, utensils, currency coins and medicines due to its brilliant metallic luster, stability in air and water and anti-bacteria and anti-fungi properties (Jain, Huang et al. 2007) (Erhardt 2003; Daniel and Astruc 2004; Brayner 2008; Maneerung, Tokura et al. 2008). In fact, noble metal is also valuable due to its unique physicochemical properties, the highest electrical and thermal conductivity, the lowest contact resistance, and the highest optical reflectivity (particularly in ultra-violet region) of all metals(Edwards and Petersen 1936 ; Hammond 2000). Its d-electron configuration endows them with active chemical properties, for example, 3 variable oxidation states for silver, the most common of which is the +1 state, as in $AgNO_3$, the +2 state as in silver(II) fluoride AgF_2, and the +3 state as in compounds such as potassium tetrafluoroargentate $K[AgF_4]$, and suitability as catalysts by losing one or two more 4d electrons (Dhar, Cao et al. 2007). Silver and gold have the stable face-centered cubic (fcc) crystal structures but readily absorbs free neutrons due to its massive nucleus, which make them good absorbers for nucleus raidation. These unique features have enabled them to be applied to diverse applications such as those mentioned above, medical and dental applications, photography, electronics, nuclear reactors, catalysts, clothing and foods (http://en.wikipedia.org/wiki/Silver).

The intrinsic features of noble metal also endow their nanoscale species with attractive physicochemical properties due to the size and shape effects, including unique optical properties (e.g. Localized Surface Plasmon Resonance: LSPR; Surface Enhanced Raman Scattering: SERS), catalytic/electric properties and bio-functions (Percival, Bowler et al. 2005; Jain, Huang et al. 2007; Schwartzberg and Zhang 2008; Zhou, Qian et al. 2008; Vo-Dinh, Wang et al. 2009). Although ancient people used some features of Ag or Au nanocolloids (e.g. optical property) in fabrication of ceramic glazes for lustrous or iridescent effect in ancient Persia, they did not realize that these effects were due to nanoscale effects from size, shape and surface morphology dependent physicochemical properties of silver materials (Erhardt 2003; Brayner 2008). As materials science has progressed down to nanoscale, the unique properties of nanoscaled noble metal materials are only now being recognized and realized intentionally. These properties have shown vast applications in

microelectronics, photonic devices, optoelectric coupling, catalytic processes, biomedical engineering and medicines. As understanding that the intrinsic properties (e.g. optical, catalytic) of nanomaterials on the size, shape, surface spatial morphology and arrangement (Ahmadi, Wang et al. 1996; Jensen, Duval Malinsky et al. 2000; Mock, Barbic et al. 2002; Haynes, Mcfarland et al. 2003; Noguez 2007; Song 2009) has increased, fabrication of silver or gold nanoparticles (NPs) and their arrays with controlled three-dimensional (3D) morphologies, interspacing and orientation has become a very significant research stream in recent years. A variety of fabrication techniques, such as thermal decomposition, metal salt reduction, photo reduction/conversion, template assisted growth and deposition, γ-ray-irridation, as well as microfluidic processes have been developed. As a result, significant progresses have been achieved in the tailoring of the 3-dimension (3D) morphologies (size, shape and surface morphology), crystal structures and spatial arrangement of noble metal nanomaterials as desired.

Template assisted (TA) lithography (LIGA) has developed to a powerful physical technique that enables the production of surface morphology confined NPs and NPs arrays with controlled shapes, sizes and interparticle spacing (Jensen, Duval Malinsky et al. 2000; Lee, Morrill et al. 2006; Zhang, Whitney et al. 2006; Lombardi, Cavallotti et al. 2007; Zhu, Li et al. 2008; Song 2009). Lots of templates have been developed for these purposes, such as porous polymers(Lombardi, Cavallotti et al. 2007), porous Al_2O_3 foils(Chong, Zheng et al. 2006; Lee, Morrill et al. 2006; Xu, Meng et al. 2009), or nanosphere arrays (polymers or ceramics)(Zhang, Whitney et al. 2006; Song 2009; Song and Elsayed-Ali 2010; Song , Zhang et al. 2011), resulting in varieties of template-assisted lithography, correspondingly as porous polymers LIGA (PP-LIGA), porous anodic Al_2O_3 LIGA (PAA-LIGA), or nanosphere-LIGA (NSL). Among them, the most popular and well-developed method may be NSL. In this chapter, recent progresses in NSL, for controlled producing noble metal nanomaterials will be summarized. The first discussion involves in this technique for size, shape and surface morphology controlled fabrication of noble metal nanoparticles (NPs) and nanoarrays. Then four distinct progresses in the development of NSL techniques: (1) Fabrication of hierarchically ordered nanowire arrays on substrates by combination of NSL and Porous anodic alumina (PAA); (2) Identification of single nanoparticles and nano-arrays by combination of NSL and multi-hierarchy arrayed micro windows; (3) Fabrication of biosensing system based on the combination of the noble metal nanoparticles and nanoarrays fabricated by NSL and microfluidic techniques; (4) Synthesis of solution-phased nanoparticles by the transfer of the surface confined NPs fabricated by NSL into solutions, will be discussed. In (2) and (3), the related 3D morphologies and arrangement dependent optical properties, and comparison between the numerical and experimental results, revealing their intrinsic quantum mechanism, such as LSPR will be analyzed. These researches are fundamental requirements for the discovery of novel properties and applications of noble metal NPs, as well as for paving the theory development. Finally, issues and perspectives in the controlled fabrication of noble metal nanomaterials by NSL, and investigation of their 3D morphologies and arrangement dependent optical properties for future potential applications will be highlighted and discussed in closing.

2. Size and shape controlled fabrication of nanomateials via NSL

Nanospheres have been used to form uniformly arranged layers as templates to produce perfect triangle nanoprisms on substrates (Haynes and van Duyne 2001; Song and Elsayed-

Ali 2010). The routine procedure for the production of triangular shaped nanoprisms, based on the nanosphere LIGA, is described in Figure 1 (a: cross-section view; b: top view) (Hulteen, Treichel et al. 1999; Haynes and van Duyne 2001; Song 2009). The hexagonal arranged nanosphere mono layer is first formed on the substrate by a coating process (e.g. dip-coating, rotating-coating or spinning-coating) (Step 1: a). The interstitials among any three adjacent nanospheres will form triangle shaped voids (Step 1: b) as templates. The desired noble metal (e.g. Ag) will then be deposited on the triangle shaped interstitials among the nanospheres to form triangle shaped Ag NPs (Step 2: a and b). After nanospheres are released by sonication or other methods, surface-confined triangular Ag nanoprisms can be obtained (Step 3: a). By this nanosphere LIGA process, uniform hexagonal-arrayed triangle nanoprisms can be fabricated on a variety of substrates (e.g. glass, mica, silica wafer, PMMA, etc.). Step 3-b is an Atomic Force Microscope (AFM) image of Ag triangular nanoprisms fabricated by our group using a self-assembled monolayer of 300 nm polystyrene nanospheres as the template (Song 2009).

The initial critical step in NSL is the formation of a uniform large scale nanosphere template. Both drop-coating or spin-coating can produce uniform templates on a glass, silica wafer or mica substrate. The uniformity of the nanosphere template produced by drop coating depends on the nanosphere type and concentration, the hydrophilic properties of the substrate, the environmental humidity and temperature, and the drying speed. A monolayer colloidal polystyrene nanosphere mask can be prepared by drop-coating of ~3.0-4.0 μL, 3-10 times diluted nanosphere solution (conc. 4.0 wt.%) onto the glass support and leaving them to dry overnight. A detailed procedure to fabricate the nanosphere mask using drop-coating is as follows. The glass substrates are cleaned by sonication with a mixture of sulfuric acid and hydrogen peroxide (3:1 = conc. H_2SO_4: 30% H_2O_2, Volume ratio) at 80 ^oC for 30 min and washed using sufficient nanopure water. Then, the glass substrates are sonicated in a mixture of ammonia and hydrogen peroxide (5:1:1 = H_2O: NH_4OH (37%): 30% H_2O_2, volume ratio) to increase the hydrophilic property on the surface of the glass substrates. Finally, the glass substrates are washed using sufficient nanopure water again and stored in the nanopure water for future use. When drop coating is to be performed, the glass substrate is picked up from the nanopure water from one of its edges. The remaining water droplets on the glass substrate are removed by touching the opposite edge on filter paper. The substrate is then left flat in a clean Petri-dish with a tilt angle of ~3-5^o. A 15 μL of PS nanosphere solution is added on the surface of the glass substrate using a droplet. The water spreads over the whole glass substrate to form a semi-ellipsoidal shaped water spot. The Petri-dish is left for enough time to allow the water to evaporate. During evaporation, the temperature is kept at 18±3 ^oC and the humidity is kept ~50±5%. In our group, a near-uniform monolayer nanosphere template can be prepared on almost the whole glass substrate (18 mm diameter). Figure 2 shows one typical area of a near-uniform monolayer template over scale ~20 μm. From the magnified image, a selected area shown in the inset, no lattice defects can be observed. Using this template, uniform Ag nanoprisms can be fabricated by vapor deposition process. One typical area fabricated by my group is shown in Step 3-b in Figure 1, where these nanoprisms have very uniform edge length of 67 ± 4 nm (STDEV% of 6%) and thickness of 20.0±1.0 nm (STDEV% of 5%) (Song 2009).

Recent progress in nanosphere lithography (NSL) has shown that it provides a good template for other shape (besides triangle) controlled fabrication of surface confined NPs by a combination of deposition angle tilting, multi-step deposition and different post treatment

methods(Haynes and van Duyne 2001; Song and Elsayed-Ali 2010). A new class of NSL structures has been fabricated by varying the deposition angle, θ_{dep}, between the nanosphere mask and the beam of material being deposited, which is hereafter referred to as angle-resolved NSL (AR NSL)(Haynes and van Duyne 2001). The size and shape of the three-fold interstices of the nanosphere mask change relative to the deposition source as a function of

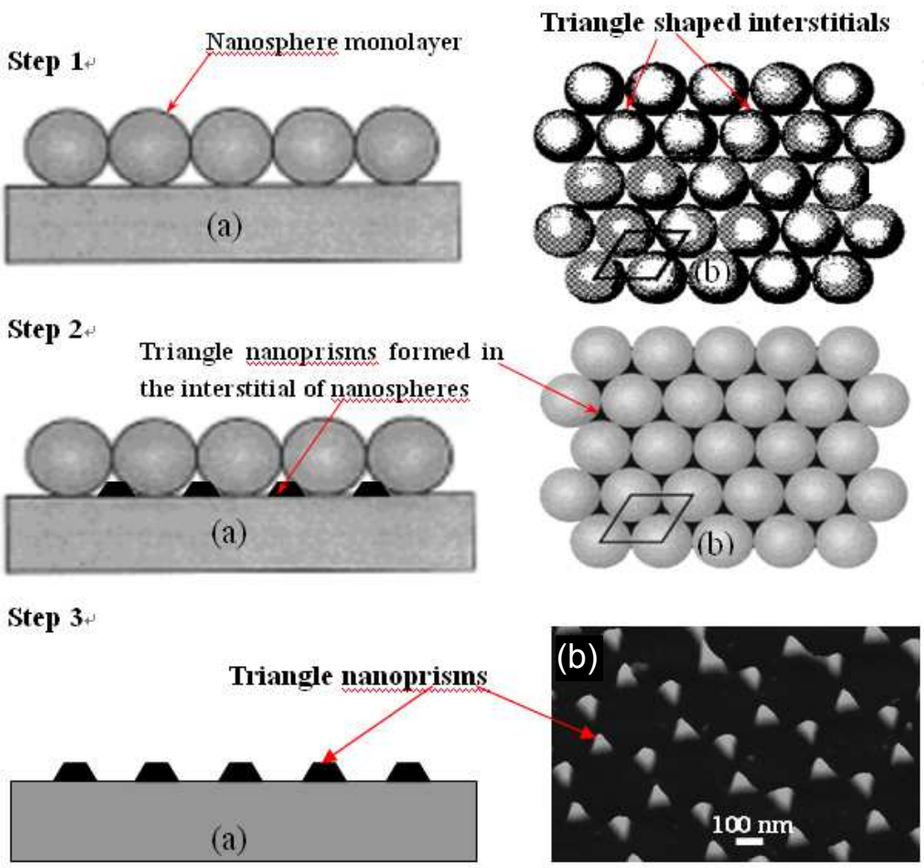

Fig. 1. The NSL process for triangular NPs fabrication. Step 1a: The hexagonal arranged nanosphere mono layer is first formed on the substrate by coating process; Step 1b: The interstitials among any three adjacent nanospheres will form triangle shaped voids as templates; Step 2a-b: the Ag metal will be deposited on the triangle shaped interstitials among the nanospheres to form triangle shaped Ag NPs; Step 3a: The nanospheres will be released by sonication or other methods, leaving the triangle shaped Ag nanoprisms on the substrates, by this nanosphere LIGA process, the hexagonal arrayed uniform triangle nanoprisms can be fabricated on variety of substrates (e.g. glass, mica, silica wafer, PMMA, etc.); Step 3b: The AFM image for Ag triangle nanoprisms fabricated by monolayer template from 290 nm polystyrene nanospheres in my group, these nanoprisms have very uniform edge length of 67 ± 4 nm (STDEV% of 6%) and thickness of 20.0 ± 1.0 nm (STDEV% of 5%). (a): cross-section view; (b) top 3D view. (Adapted in part from Song, Y. China Patent, CN200910085973.9; Haynes, C. L.; van Duyne, R. P., *J. Phys. Chem. B* 2001 105, 5599, Figure 2, Copyright (2001) American Chemical Society; and Hulteen, J. C.; et al., *J. Phys. Chem. B* **1999** 103, 3854, Figure 1, Copyright (1999) American Chemical Society.)

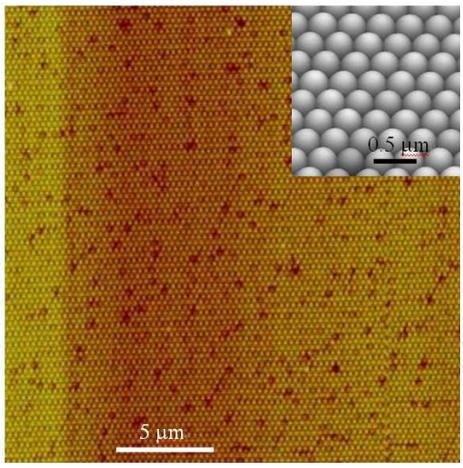

Fig. 2. Nanosphere templates based on 290 nm spherical polystyrene nanospheres for Ag nanoparticle fabrication (Reprinted from Song et al., Appl. Surf. Sci. 2010 256, (20), 5961, Figure 1. Copyright (2010) Elsevier.).

θ_{dep}, and accordingly, the deposited nanoparticles' shape and size are controlled directly by θ_{dep} and the diameter of nanosphere. Figure 3 schematically describes the effect of angle-resolved deposition on the interstices of a NSL mask from the top view. (Figure 3). As a convention, $\theta_{dep} = 0^o$ represents a substrate mounted normal to the evaporation beam (Figure 3A), and all variations of θ_{dep} are made by mounting the substrates on machined aluminum blocks. It is clear from this illustration that an increase in θ_{dep} causes the projections of the interstices onto the substrate to decrease and shift (Figure 3B and 3C). At high values of θ_{dep} (e.g. 45^o, Figure 3C), the projections of the interstices close, completely blocking the substrate to line of sight deposition.

One very important consequence of AR NSL, beyond the increased flexibility in nanostructure architecture, lies in the decrease in nanoparticle size. Before AR NSL, the only way to fabricate nanoparticles in the 1-20 nm size range with NSL required self-assembly of nanospheres with diameters on the order of 5-100 nm. Not only synthesis of uniform nanospheres at this range is usually difficult, but self-assembly of such small nanospheres into well ordered 2D arrays is extremely challenging because of problems with greater polydispersity and the surface roughness of substrates. However, with AR NSL, increasing θ_{dep} from 0^o to 20^o will halve the in-plane dimension of nanosphere templates, leading to the success in small nanoparticle preparation by NSL. In addition, nano-overlapped, nano-gapped and nano-chained structures can be addressed by multi-step AR NSL, which is fulfilled by depositing materials through a nanosphere mask mounted at different θ_{dep} below the overlap threshold value of θ_{dep} several times. Van Duyne et al have used two step AR NSL to fabricate over-lapped and gapped Ag nanostructures through a nanosphere mask with D = 542 nm onto mica substrates by a first deposition at $\theta_{dep} = 0^o$ and a second deposition at an increased θ_{dep}. The importance in the fabrication of over-lapped nanoparticles theoretically exists in the enhanced optical properties due to their increased aspect ratio (in-plane width/out-of-plane height) nanoparticles(Kreibig and Vollmer 1995). Nano-overlapped structures can give an significantly increased sensitivity of optical response since they allow predictable aspect ratio to increase up to double of the original value (Haynes and van Duyne 2001). One of the interests for gapped nanostructures may exist in the investigation of the distance dependent LSPR coupling amomng gapped nanostructures.

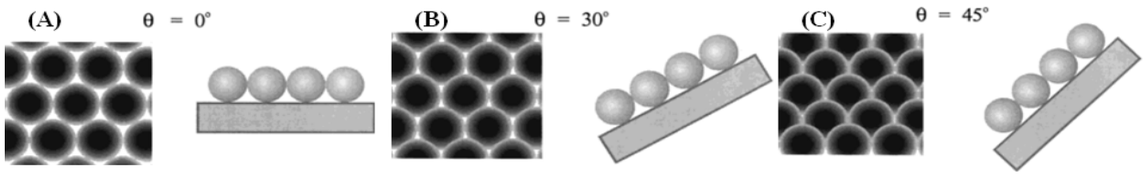

Fig. 3. Scheme of the angle resolved deposition process. (A) Samples viewed at 0º. The interstices in the nanosphere mask are equally spaced and of equal size. (B) Sample viewed at 30º. The interstices in the nanosphere mask follow a pattern including two different interparticle spacing values, and the interstitial area is smaller. (C) Sample viewed at 45º. The interstices are now closed to line of sight deposition. (Adapted from Haynes, C. L.; van Duyne, R. P., *J. Phys. Chem. B* 2001 105, 5599, Figure 5, Copyright (2001) Amercian Chemical Society.)

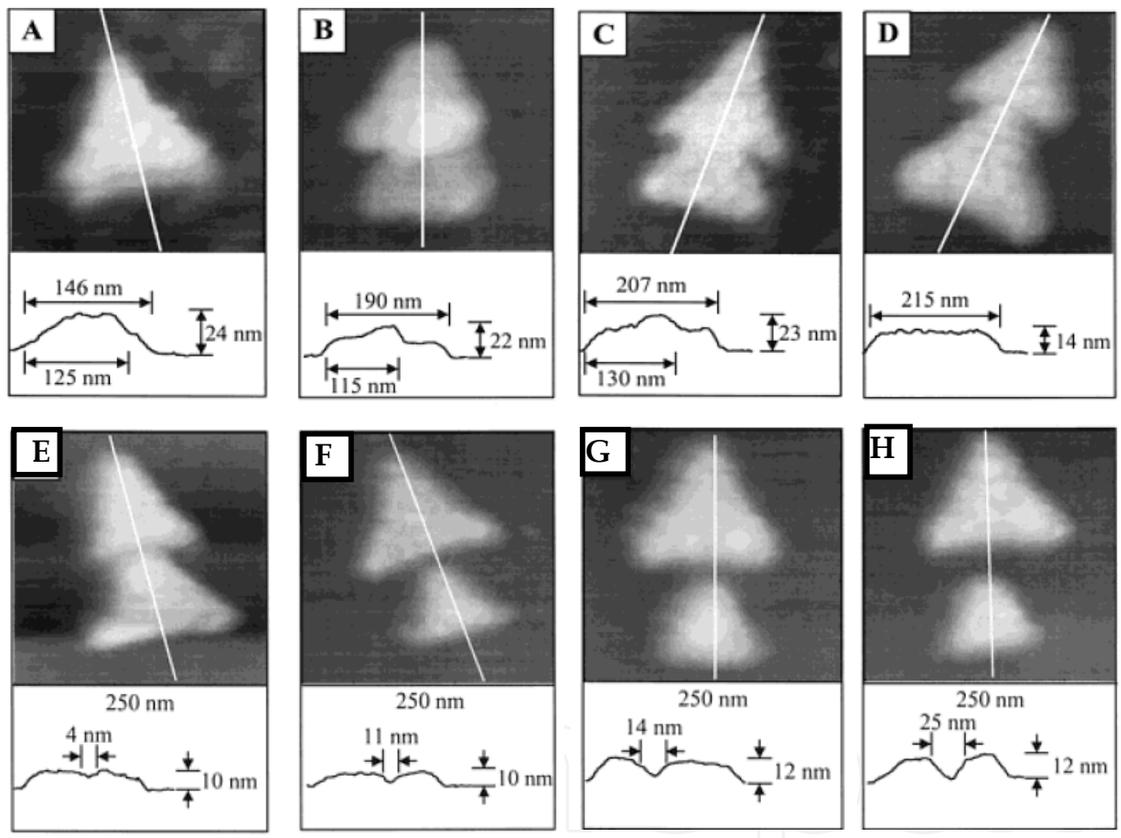

Fig. 4. Contact mode AFM images of typical Ag nano-overlapped and nano-gapped structures fabricated on mica substrates using the single layer nanosphere template. (A) 300 nm - 300 nm image, D = 542 nm, dm = 20 nm, θ_{dep} = 0 º and 6 º. (B) 250 nm - 250 nm image, D = 542 nm, dm = 20 nm, θ_{dep} = 0 º and 10 º. (C) 300 nm - 300 nm image, D = 542 nm, dm = 20 nm, θ_{dep} = 0° and 15º. (D) 250 nm-250 nm image, D = 542 nm, dm = 20 nm, θ_{dep} = 0° and 20 º. (E) 250 nm - 250 nm image, D = 542 nm, dm = 20 nm, θ_{dep} = 0° and 22 º. (F) 250 nm - 250 nm image, D = 542 nm, dm = 20 nm, θ_{dep} = 0° and 23 º. (G) 250 nm - 250 nm image, D = 542 nm, dm = 20 nm, θ_{dep} = 0° and 24 º. (H) 250 nm - 250 nm image, D = 542 nm, dm = 20 nm, θ_{dep} = 0° and 26 º. (Adapted from Haynes, C. L.; van Duyne, R. P., N *J. Phys. Chem. B* 2001 105, 5599, Figure 6 and Figure 7, Copyright (2001) Amercian Chemical Society.)

The overlap percent of nanoparticles can be adjusted by θ_{dep} at a certain mass deposition thickness (e.g. 20 nm) and nanosphere diameter (e.g. 542 nm). As shown in Figure 4A-D, the overlap percent decreases with the increase of θ_{dep} from 0^o to 20^o. The θ_{dep} at 20^o is the threshold deposition angle since neither overlap nor gap is visible by AFM investigation at this point (Figure 4D). When the second deposition angle is more than the threshold angle (e.g. 20 ^{o} based on the fabrication condition using nanosphere mask with D = 542 nm and mass thickness d_m = 20 nm(Haynes and van Duyne 2001)), nano-gapped structures can be formed. With the same experimental parameters defined above, the gap between nanoparticles increases as θ_{dep} is increased from 22^o to higher values up to thecritical θ_{dep} value at which the interstitial projections are closed to line-of-sight deposition. Figure 4E-H shows the AFM images of the typical nano-gapped Ag structures with different gap distances when the second deposition angles change from 22^o, to 23^o, to 24^o and to 26^o. Another of the applications proposed by van Duyne is to use the nanogap architecture to measure the electrical conductivity of a single molecule or nanoparticle (Haynes and van Duyne 2001). If one side of the nanogap is insulated from a conductive substrate while the other side of the nanogap is in contact with a conductive substrate, the conductance of the junction should be measurable with a scanning tunneling microscopy probe.

Clearly, like the two depositions at different values of θ_{dep}, three or more depositions will further extend the range of nanoparticle architectures accessible by AR NSL. An endless number of nanostructures are possible when one combines the ability to vary θ_{dep} and to perform multiple material depositions. As an example, the nanochain motif with three-connected-nanoparticle chains can be fabricated by three consecutive depositions. The first deposition is done at $\theta_{dep} = -15^0$, whereas the second and third depositions will be further done at $\theta_{dep} = 0^o$ (tilted forward) and $\theta_{dep} = 15^o$ (tilted backward). An AFM image of the nanochain structure is shown in Figure 5 and gives a typical domain where the sample tilt axis is aligned with the triangular base of the nanoparticles. Possible applications of the nanochain architecture include sub-100 nm near-field optical waveguides, chemical and biological sensors based on the LSPR of these high aspect ratio nanoparticles, and the fabrication of nanowires.

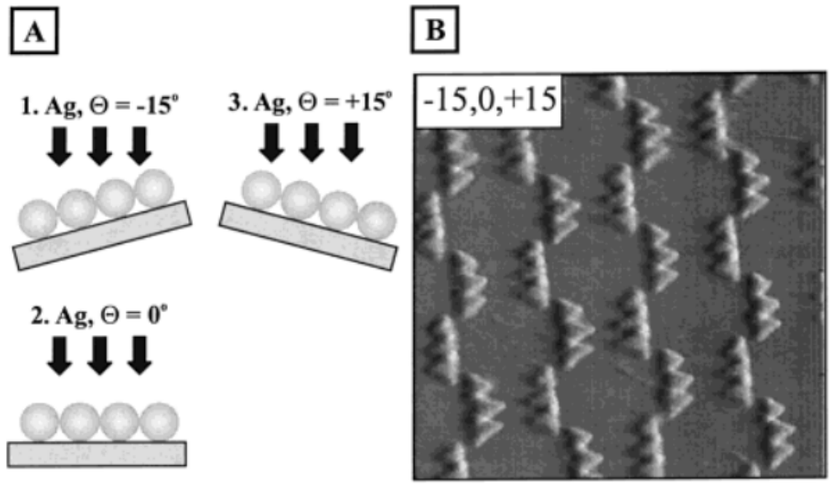

Fig. 5. (A) Schematic fabrication process and (B) contact mode AFM image for three deposition nanochain structure on mica. 1.6 μm - 1.6μm area, D = 542 nm, dm = 10 nm, θ_{dep} = +15°, 0°, and -15°. (Reprinted from Haynes, C. L.; van Duyne, R. P., *J. Phys. Chem. B* 2001 105, 5599, Figure 9, Copyright (2001) Amercian Chemical Society.)

We recently developed a modified NSL process to fabricate Ag NPs with controlled shapes on substrates. The modification in NSL is performed by thermally annealing the triangular nanoprisms, and sonication to remove weak tips, followed by removing debris and small broken parts around the NPs on the substrates(Song and Elsayed-Ali 2010). The detailed process is shown in the following: (1) Releasing the nanospheres by immersing the cover slip into a 5% HCl solution for 30 minutes, then immersing the glass substrates into CH_2Cl_2 for 30 s, then sonication for ~20-60 s; (2) The fabricated Ag nanoprisms on the glass substrates are annealed at 100-300 ^oC for 2-5 hours; (3) Then Ag nanoprisms are cleaned by immersing the glass cover slip into 5% HNO_3 for 10-20 s to remove any surface contamination and dissolve debris around the NPs, and then washed by large amount of nanopure water. Comparing the AFM images in Step 3-b of Figure 1 showing the NPs without above post treatment, tip-rounded triangle nanoprisms, square-shaped and trapezoidal Ag NPs (Figure 6) can be obtained via one or two of the above treatment. We observe that thermal annealing results in much more uniform NP surfaces without the thin, weak tips and edges (Figure 6(a-1)). From the magnified AFM plane image in the inset of Fig. 6(a-1) and the 3D image in Figure 6(a-2), the NPs still show triangular prism shape with

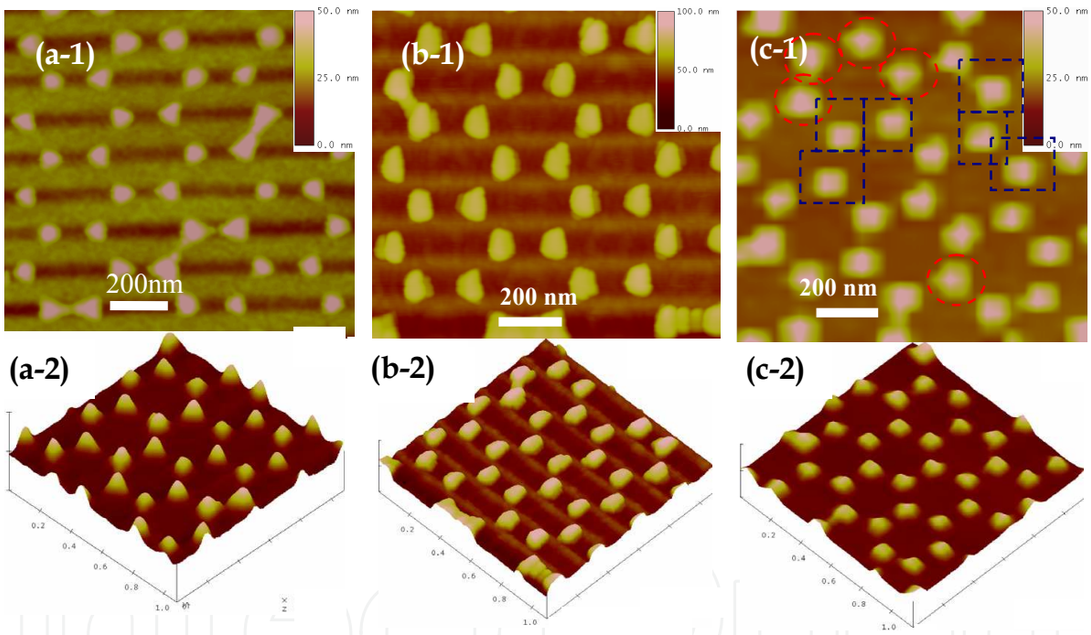

Fig. 6. Surface-confined Ag NPs with controlled shapes fabricated by the modified NSL process. (a-1) AFM image of triangular prism Ag NPs with rounded tips after thermal annealing at 200 ^oC for 4 hours, cleaning by 5% nitric acid, and washing by nanopure water. (a-2) The 3D image of the triangular prism Ag NPs with rounded tips. (b-1) Flat trapezoidal Ag NPs after sonication to remove one tip, thermal annealing, cleaning by 5% nitric acid, and washing by nanopure water. (b-2) The 3D image of the trapezoidal Ag NPs with one snipped tip. (c-1) The quadrilateral or pentagon shaped Ag NPs after sonication intensively to remove two tips, thermal annealing, cleaning by 5% nitric acid and washing by nanopure water. Dashed circles: pentagonal Ag NPs with one sharp tip left; dashed squares: quadrilateral Ag NPs. (c-2) is the 3D image of the quadrilateral and pentagon shaped Ag NPs. (Song Y.; Elsayed-Ali H. E., Appl. Surf. Sci. 2010 256, (20), 5961, Figure 3, Copyright (2010) Elsevier.)

rounded edges and little surface defects. Alternatively, if we sonicate the NPs produced by NSL for ~30-45 s to remove a weak tip, anneal them at 200 ºC for 1- 4 hours, then wash them with 5% nitric acid, trapezoidal shaped NPs with rounded edges are formed, as shown in Figure 6(b-1) and 6(b-2). If the sonication time is increased to more than 2 min, the NPs lose their two sharp tips and form quadrilateral or pentagon shaped NPs. After thermal annealing for 1-4 hours and washing with 5% nitric acid, their edges and corners become rounded, as shown in Fig. 6(c-1), which show quadrilateral NPs (in dashed squares) or pentagon (in dashed circles). The 3D AFM image, Figure 6(c-2), shows that these NPs have rounded edges and corners. Clearly, even after thermal annealing, they are still showing prism shapes with increased thickness from their edges to centers according to their 3D AFM images.

The work described above demonstrates that NSL, broadly defined to include AR NSL and some modified post treatment after deposition of the desired materials, is manifestly capable of creating far more than arrays of nanotriangles, nanodots as previously supposed. The progresses in NSL endow much potential in the size and shape controlled fabrication of nanoparticles and nanoarrays, which gives NSL a bright future since the ability of NSL to synthesize monodisperse, size- and shape- tunable nanoparticles can be exploited to precisely investigate the size- and shape- dependent physiochemical properties of nano-optics and nanoarrays.

3. Investigation of optical properties of specific noble metal nanoparticles and nanoarrays by the combination of NSL and multi-hierarchy arrayed micro windows

The physicochemical properties of nanomaterials significantly depend on their three-dimensional (3D) morphologies (sizes, shapes and surface topography), their surrounding media, and their spatial arrangement. Systematically and precisely correlating these parameters with the related physicochemical properties of specific single nanoparticles (NPs) or nanoarrays is a fundamental requirement for the discovery of their novel properties and applications, as well as for advancing the fundamental and practical knowledge required for the design and fabrication of new materials(Song , Zhang et al. 2011). The lack of effective means of fabricating recognizable 3D morphologies controlled NPs and nanoarrays and correlating their structure parameters with their physicochemical properties as observed by different characterization techniques represents an obstacle for studying the 3D morphology-dependent properties of individual NPs and nanoarrays(Song, Zhang et al. 2011). Most current studies investigate the physicochemical properties of the NP ensemble, but not of a single NP(Jin, Cao et al. 2001; Kelly, Coronado et al. 2003; Haes, Zou et al. 2004; Song , Zhang et al. 2011). The ensemble of NPs is typically heterogeneous, because the morphologies of individual NPs prepared by routine chemical synthesis or physical vapor fabrication methods are rarely identical at the nanometre or sub-nanometre scale (Song , Zhang et al. 2011). Effective methods for 3D morphology controlled fabrication of nanomaterials, and to correlate their 3D morphology of single NPs or nanoarrays with their physicochemical properties are also essential to address fundamental and practical questions related to the single NPs (Song , Zhang et al. 2011).

An important research area in nanoscale plasmonic optics is single NP identification and characterization of their 3D morphologies and space-orientation dependent physicochemical

properties(Yang, Matsubara et al. 2007; Song 2009; Song , Zhang et al. 2011). Recently, much attention has been given to the localized surface plasmon resonance (LSPR) of metal NPs because of their promising applications in plasmonic circuits, optoelectronic transducers, optical bioprobes, and surface plasmon resonance interference lithography(Shen, Friend et al. 2000; Prasad 2004; Ozbay 2006; Song 2009; Song , Henry et al. 2009; Song , Jin et al. 2010; Song, Sun et al. 2010; Song , Zhang et al. 2011). Since the plasmonic properties of metal NPs intrinsically rely on their size, shape, surface topography, crystal structure, inter-particle spacing and the dielectric environment around them, methods to correlate their plasmonic properties with the above structural and environmental parameters have become one of the most rapidly developing research directions (Song , Zhang et al. 2011).

In the precise investigation of the relationship between the LSPR properties and their 3D morphologies of specific nanoparticles and nanoarrays, two kinds of methods have been developed recently, or the *in situ* method and the spatial-localization method (Song , Zhang et al. 2011). The *in situ* method combines at least two different instruments together to conduct the structure and property characterization simultaneously: one can be used to characterize the 3D morphology (e.g. AFM or STEM) of NPs and the others will be used to chatacteize the LSPR-related optical properties of the same NPs (e.g. Dark-field microscope and spectroscopy). The spatial-localization method requires using markers to recoganize the same single nanoparticle in different instruments. We have also developed one spatial-localization method to precisely investigate the 3D morphologies dependent LSPR properties of specific NPs and nanoarrays by the combination of NSL and traditional UV-LIGA, where Ag NPs and nanoarrays can be fabricated by NSL in the pre-formed multi-hierarchy arrayed transparent micro-windows on the substrates (e.g., glass cover slip) by the UV-LIGA(Song 2009; Song , Zhang et al. 2011). This technique permits easy characterization of the 3D morphologies of single NPs by AFM or SEM and their LSPR spectra using dark-field optical microscopy and spectroscopy (DFOMS). It is also possible to investigate the local morphology dependence of the LSPR spectra of the single NPs and nanoarrays. In this method, multi-hierarchy arrayed micro windows are first fabricated on a glass cover slip using the standard photolithography, whose details are shown in reference 27. Fig. 7A and Fig. 7B show one example of the designed multi-hierarchy arrayed micro windows (3 tiers) and the typical final micro-windows (Fig. 7C) pattern after printing. The multi-hierarchy arrayed micro-windows on the glass cover slip are used to identify the location and orientation of single NPs, whose tiers can be determined by the observed field at desired resolution. For example, in the first tier of the multi-hierarchy arrayed micro windows (Fig. 7A), each local area can be discerned by marking its X and Y number, such as the shaded area X1–Y2. Then, in the second tier of the multi-hierarchy arrayed micro windows (Fig. 7B), the scale can be reduced by M or N times and each local area can also be marked by x and y number. If this area is the sub-tier in the shaded area of the first tier, it can be labeled as X1–Y2–x3–y3. In a similar way, step-by-step, we can reach the last tier with several transparent micro windows available (Fig. 7C), in which the desired nanoparticle can be made by different fabrication methods (e.g., electron beam lithography or nanosphere lithography). Nanoparticles less than 10 nm of different shapes synthesized by a wet-chemical process can be immobilized by a routine diluted deposition process. Consequently, the same nanoparticle in each window can be identified by comparing the images taken by the optical microscope with those characterized by the AFM. Finally, in each window, the same nanoparticle can be characterized by different techniques (e.g., DFOMS and AFM) allowing correlation of its 3D morphology with its optical response(Song 2009; Song , Zhang et al. 2011).

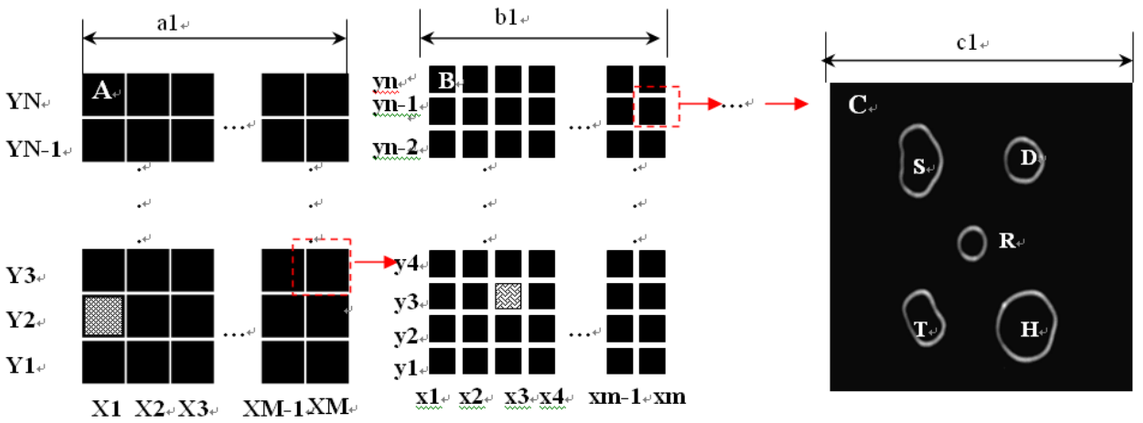

Fig. 7. The multi-hierarchy arrayed micro windows on the substrate (e.g., glass cover slip). (a) The first tier of the multi-hierarchy arrayed micro window, each local area can be discerned by marking its X and Y number, such as the red-dashed square area of X1–Y2. (b) The second tier of the multi-hierarchy arrayed micro windows, whose scale can be reduced by M or N times, whose local area can also be marked by x and y numbers. If this net area is the sub-tier n the red area of the first tier, it can be labeled as X1–Y2–x3–y3. Step-by-step, the last tier with several unique-shaped transparent windows can be reached. The open windows can be made with different shapes. (c) The nanoparticles can be fabricated on the micro-pattern by various methods (e.g., nanosphere lithography). In each window, the same nanoparticle can be identified by comparing the images taken by optical microscopy, AFM, or other microscopy methods. Finally, the structural parameters (size, shape, orientation, interparticle spacing, and thickness) can be correlated with their optical responses (Reprinted from Song Y.; et al., Nanoscale 2011, 3, 31-44, Figure 7, copyright (2011) from the Royal Society of Chemistry.)

A typical example to identify NPs and nanoarrays using both AFM and DFOMS is illustrated in Figure 8. Triangular Ag NPs and hexagon-arranged nanoarrays fabricated on the surface of glass cover slips within the nearly circle-shaped micro window can be identified and characterized using AFM (Figure 8A, 8B is the 3D AFM image of the dash-squared area in 8A) and DFOMS equipped with a color camera (Figure 8 C) and charge-coupled device (CCD) camera (Figure 8D). The CCD camera offers higher spatial resolution than the color camera, while the color camera provides the real colors of individual Ag NPs that are generated by LSPR. The center of each individual NP in the optical images recorded by the CCD is located with a single-pixel resolution (each pixel can be 125 nm or 67 nm depending on the CCD resolution and equipment setup) by determining the address of the pixel with the highest intensity of the NP. The positions of individual NPs of interest (e.g. the circled one) within the micro window in the optical images (Figure 8C and D) are then determined with a spatial resolution limited by the optical diffraction limit (~200 nm) and an orientation angle resolution of about 1.0 degree. This approach allows us to correlate AFM images of individual NPs (as the one circled in each image) with the same NP shown in its corresponding optical image and to investigate its 3D morphological-dependent LSPR properties. Clearly, these triangle nanoparticles in this window almost show the same scattering color (Figure 8C) and intensity contrast (Figure 8D). By comparing their scattering color images (Figure 8C) with their AFM images (Figure 8A and B) of these nanoparticles, it

is once again showing that NSL is powerful method in the fabrication of uniform triangular nanoparticles and nanoarrays.

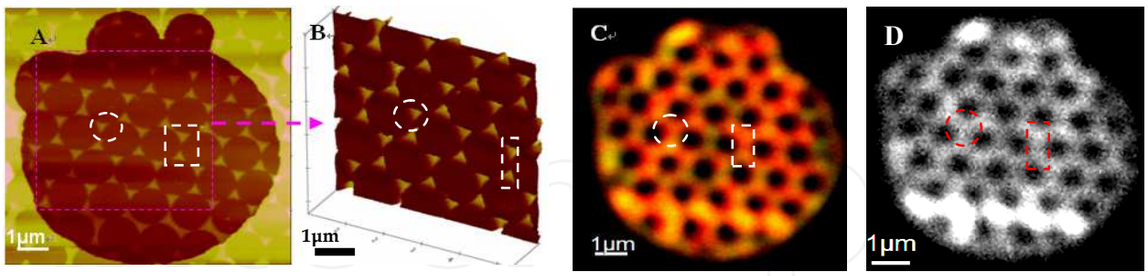

Fig. 8. One example for the identification of the specific nanoparticles and nanoarrays in different instruments via multi-hierarchy arrayed micro windows based on Ag triangle nanoparticles and nanoarrays fabricated by NSL in one nearly circle-shaped window. (A) The plan view of the hexagon-arrayed triangle Ag NPs in one circle micro-window scanned by atomic force microscope (AFM); (B) the 3D view of the hexagon-arrayed triangle Ag NPs marked in the large pink dash-square in (A); (C) the real scattering color of these hexagon-arrayed triangle Ag NPs observed under a dark-field microscope; (D) the CCD images of the scattering light of these hexagon-arrayed triangle Ag NPs recorded by a CCD camera equipped in the dark-field microscope. The dashed circles in each image refer to the same specific particle and the dashed squares in each image refer to the same specific nanoparticle pair. (Adapted from reference Y. Song, China Patent, Appl. No. CN200910085973.9).

We have used it to investigate size- and shape-dependent LSPR spectra of single Ag NPs by the analysis of the experimental results with the theoretical calculation (i.e. DDA simulation)(Song , Zhang et al. 2011). Figure 9 gives the AFM images of one specific triangle-shaped Ag NPs characterized by multi-hierarchy arrayed micro windows. The AFM image of the triangular silver NP shows that it has the edge length of 375-420 nm (Figure 9A) and the out-of-plane height of about 16.1 nm (Figure 9B). This NP shows multi LSPR scattering colors (Figure 9C), as further evidenced by its multi-mode LSPR peaks at 562.3 nm, 659.9 nm and 759.6 nm (Figure 9D-b). The peak wavelengths, peak ratios, and line widths (FWHM) at 562.3 nm and 659.9 nm from experiment are in good agreement with DDA simulation for its LSPR scattering (Figure9D-c), as have been summarized together with other shaped nanoparticles fabricated by the modified NSL in reference 27. In general, the DDA simulation shows best agreement with the experimental spectra for NPs, hence their shapes can be accurately modeled. However, it can also be seen that for wavelengths longer than 650 nm for the investigated NPs, the experimental result has a lower intensity than the simulation(Song , Zhang et al. 2011). By analysis the instrument errors and the wavelength dependent CCD quantum efficiency, these deviations are deduced by the precision in the shape construction during DDA simulations. From these results, it was also found that when the shapes and 3D morphologies of the NPs became more complicated, the deviation between the DDA simulation and the experimental result increased (Song , Zhang et al. 2011). This is due to the geometrical deviation between the real NPs and the regular species used in the calculations. If these two instrumental factors and the geometrical deviation of NPs are considered, the corrected experimental results will match with the DDA simulation very well. This result also confirms that our experimental method (DFOMS), based on the far field detection, preserves the ability to detect the near-field LSPR signal.

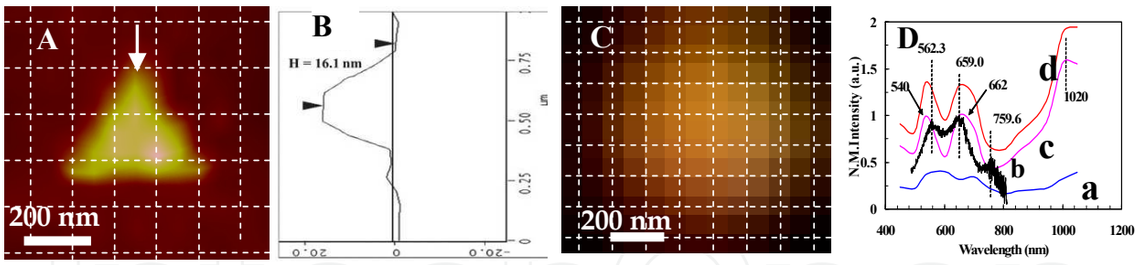

Fig. 9. (A): The AFM image for one single triangular shaped Ag nanoparticle with edge length of 375-420 nm; (B) the height mapping of the triangle shape Ag nanoparticle along the direction of the arrow in Fig. 9(A), showing the out-of-plane height of this nanoparticle of 16.1 nm; (C) the real scattering color image of this triangular shaped Ag nanoparticle; (D-a): the LSPR absorption spectrum of this nanoparticle by DDA; (D-b) the LSPR scattering by experiment; (D-c) the LSPR scattering by DDA; (D-d): the LSPR extinction by DDA. In order to identify the location and the orientation of these positions around the NPs, the AFM image and color image were netted by dashed lines with each square unit of 125 nm ×125 nm after their distances and orientations were corrected. (Adapted from references: Y. Song, China Patent, Appl. No. CN200910085973.9; Song Y.; et al., Nanoscale 2011, 3, 31-44, Figure 13, copyright (2011) from the Royal Society of Chemistry. Adapted with permission.).

This combined method based on the NSL and the multi-hierarchy arrayed micro windows also allows us to investigate the 3D morphology dependent tip-tip LSPR coupling of triangular nanoparticle pairs. The zoom-in AFM image for the detailed 3D morphology of one typical Ag nanoprism pair is shown in Figure 10A. The nanoprisms have almost the same edge size ~ 375 nm and maximum out-of-plane height ~ 17.1 nm shown in Figure 10B by the typical height map along the arrowed tip-tip direction in Figure 10A. The real scattered color for the nanoprism pair, taken from dark-field microscopy, is shown in Figure 10C. Both of the nanoprisms in the pair give red color with different brightness, which might be due to variation in their surface roughness, slightly difference in the underlying surrounding dielectrics, and the focusing distance during image recording. The middle area between the two nanoprisms clearly shows more reddish color than the optical centers of the two nanoprisms. The LSPR spectrum for the middle area of the two optical centers (representing the tip-tip-coupling) is recorded in Figure 10D using their CCD image (not shown here) for the location identification, together with that obtained by the discrete dipole approximation (DDA) calculation of the nanoprism pair. According to its 3D morphology of the nanoparticle pair, the two nanoprisms can be treated as regular triangular nanoprisms with the bottom edge length of 375 nm, the top edge length of 125 nm and out-of-plane height of 17.1 nm for conducting the DDA calculation of the nanoprism pair. The recorded LSPR spectrum (Figure 10D: a) at the middle optical center of the two nanoprisms shows three distinct peaks, one strongest peak at 605 nm, one shoulder at 536 nm, and one secondary strong peak at 754 nm. By comparing the experimental result for the tip-tip coupling of the nanoprism pair with the DDA calculation (Figure 10D: b), it can be deduced that the peak at 605 nm represents the in-plane quadrupole resonances originated from the two source nanoprisms and the peak at 536 nm is from the out-of-plane quadrapole resonances of the two source nanoprisms. Although the DDA simulation does not show one distinct peak at 754 nm, our experiment result suggest one strong peak at this wavelength, which is probably from the strong tip-tip coupling. In order to reveal whether the peak at 754 nm is mainly from the tip-tip coupling or not, the LSPR spectra from the optical centers

of the source nanoprisms, are recorded (not shown here), showing one strong peak at the same position. Generally, one can see that the peak positions and shape resonances for the two nanoprisms are almost the same, suggesting that the nanosphere lithography process is very powerful in the fabrication of the nanoprisms with almost identical 3D morphologies and surroundings. Both of the two triangle nanoprisms do not give the peak at 754 nm as strong as the pair, confirming that the additional peak at 754 nm indeed is from the tip-tip coupling. However, previous investigations did not show additional strong peak due to tip-tip coupling (Su, Wei et al. 2003; Zhao, Kelly et al. 2003). The reason for this significant coupling between the nanopair may be caused by the unique size of our particles that is just lying in the range of half wavelength of visible light, which can cause a strong long-range electrodynamic interaction among light and the collective electrons on the particle surfaces.

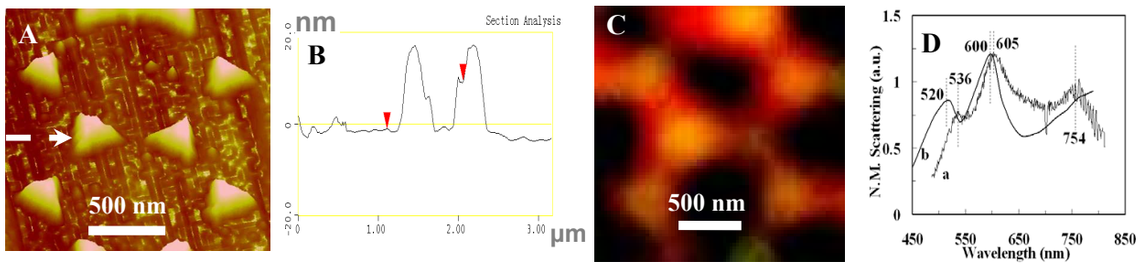

Fig. 10. Tip-tip coupling of one typical pair of triangular Ag nanoprisms in the arrays with interspacing of 103 nm is characterized using (A) AFM; (B) the scan of out-of-plane height of the two nanoprisms along the arrow direction in (A); (C) the color image taken from dark-field microscopy; (D: a) the LSPR scattering spectrum at the central locations (3 pixels) of the source nanoprisms and (D:b) the LSPR scattering spectrum of the pair calculated by DDA.

In additon, our experimental observations show that nanoprism coupling does not affect the quadrupole mode in LSPR significantly, resulting in little shifts in the highest peak at 598-605 nm (the in-plane quadrupole mode). However, one additional peak (i.e. 754 nm) as compared with the in-plane quadrupole mode can be observed. This peak resulted from LSPR coupling is in good agreement with the prediction by the semianalytical model by Schatz et al. (Zhao, Kelly et al. 2003) In the present study, the edge lengths of the triangular nanoprisms are more than $\lambda/2\pi$ (64-128 nm), which is more than the critical scale in the semianalytical model in the DDA.(Zhao, Kelly et al. 2003) Therefore, the long-range electrodynamic interaction, not electrostatic effects, will be dominant in the LSPR of the two nanoparsms. The center-to-center interspacing of the two nanoprisms is ~ 532 nm, more than the critical interspacing. As a consequence, the coupling will be mainly dertermined by the long-range radiative dipolar interactions (or radiative damping effects),(Zhao, Kelly et al. 2003) and phase retardance effects,(Su, Wei et al. 2003) resulting in one new peak with wavelength more than the highest peak for the two nanoprisms.

Based on this combined method, we have investigated the distance dependent tip-tip coupling between triangular Ag nanoprism pairs with dimensions at the range of half wavelength of visible light and distance ranging from 100 nm to 400 nm. It has been found that the coupling peak wavelength increases and the coupling intensity decreases with the increased tip-tip distance, and finally the coupling disappears (no coupling peak) when the

tip-tip distance is more than about 400 nm due to the coupling intensity becomes extremely low.

Generally, the combination of NSL and the multi-hierarchy arrayed micro windows fabricated by the routine UV-LIGA shows a powerful ability not only in the identification of nanoparticles and nanoarrays but also in the precise investigation of the fundamental theory related to the 3D morphology dependent LSPR and LSPR coupling. In our study, the detector is far-field while the DDA calculation is based on the near-field. Thereby, the results indicate that the near-field LSPR of single NPs and the coupling signals of nanoarrays can be detected by the far-field detector if the 3D morphologies of NPs or nanoarrays can be precisely accounted for in the DDA model.

4. Microfluidic biosensing system based on NSL and microfluidic reactor fabrication

Recently, Song has developed a high-throughput single Ag NPs biosensing device by coupling a variety of functionalized Ag NPs fabricated by NSL into a series of microfluidic channels (Song 2009). The designed microfluidic biosensing system based on Ag single nanoparticles and nanoparticle arrays is illustrated in Figure 11. Samples were fabricated by the combination of NSL and the traditional UV-LIGA process for the microfluidic reactor fabrication (Song 2009; Song 2010; Song and Elsayed-Ali 2010). In this biosensing system, the corresponding microfluidic channels are fabricated on the designed patterns where series of single Ag NPs or arrays (Figure 11: a) have been fabricated by careful alignment. The glass cover is then connected with glass optical fiber binding on the top of the microfluidic channels after careful alignment with the desired single Ag NPs or nanoarrays. In order to alleviate the non-specific absorption in the microfluidic channels, the channels are modified by polyvinylacholol (PVA) or polyethylene glycol (PEG) solution. After that, the single Ag NPs will be surface modified by a mixture of at least two thiol compounds with one having carboxyl group or amine group as the conjugating compound (e.g. 11-mercaptoundecanoic acid: MUA), and another thiol compound without carboxyl group or amine group as spacer (e.g. 6-mercapto-1-hexanol: 6-MCH, 1-octanethiol: 1-OT). The modification reaction is shown in equation (1). The Ag NPs can then be functionalized with biomolecules, as reporter (e.g. IgG), by a conventional 1-ethyl-3-(3- dimethylaminopropyl)-carbodiimide (EDC) coupling process to form the f, as shown in equation (2) and (3) for the functionalization of Ag NPs (Figure 11: a and b).

The number per Ag NPs can be controlled by the ratio of the conjugation compounds and spacers, which can be used to calculate the number of the responding biomolecules (e.g. Protein A) that can bind with the reporters, which can be directly sensed by the LSPR peak shift. As shown in Figure 11, the solution having a specific concentration of the corresponding detected biomolecules can be delivered into the microfluidic channels (Figure 11: g). The channel widths are designed from several hundreds micro meter to ten micrometers that will play a role like a dark-field condenser for incident white light. The scattering color changes and the LSPR spectrum variations of Ag NPs (a) caused by the binding of the detected biomolecules on the reporters, (b) will be collected in the opened windows, (d) and transported into the detector and analyzer, (f) by the glass fiber, (e) after signal magnification.

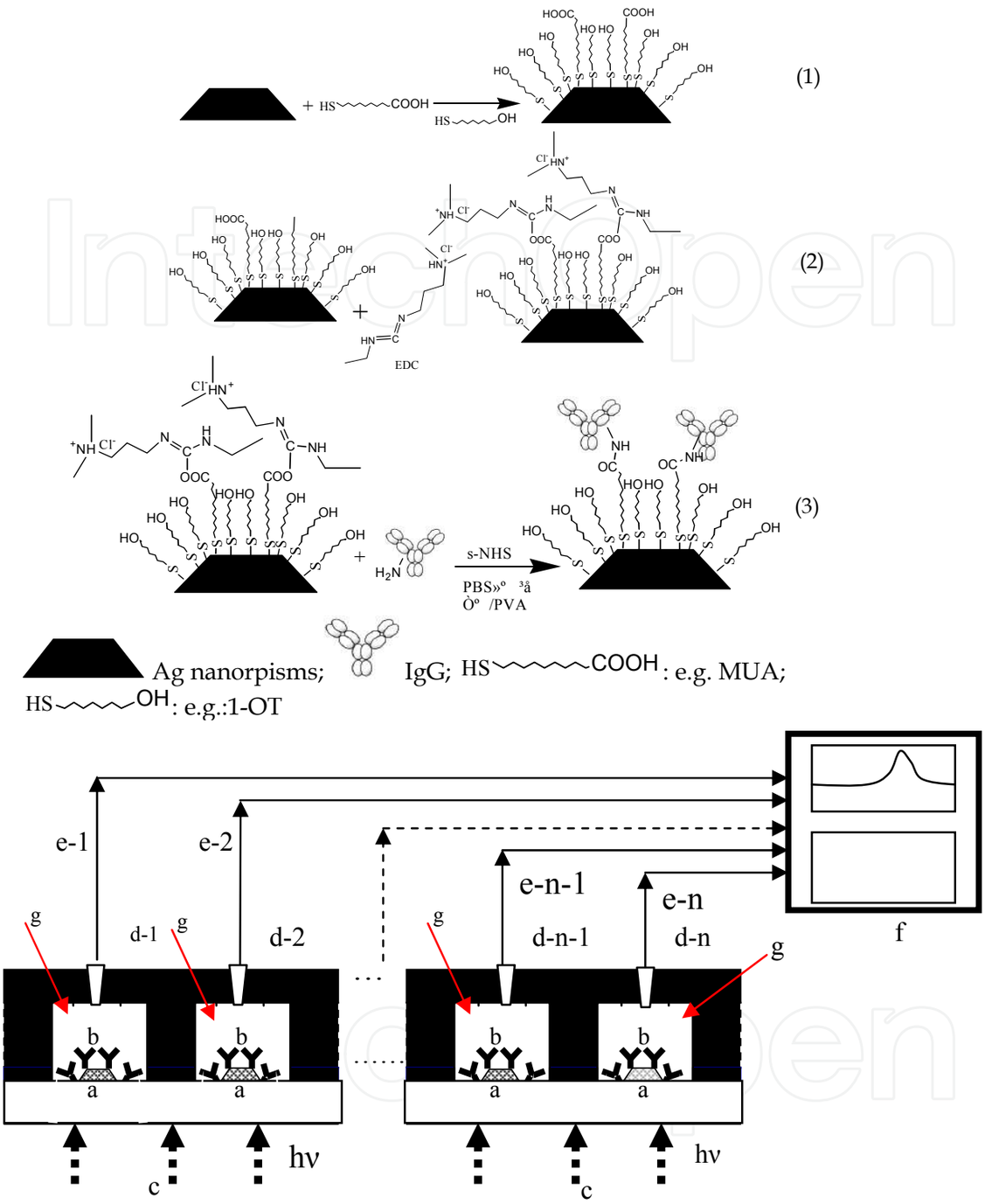

Fig. 11. a: nanoparticles (e.g. triangular Ag NPs); b: biomolecule (e.g. antibody); c: induced light (e.g. white light from tungsten lamp); d-1 - d-n)：Series of detecting windows connecting with optical microfibers in different microchannels；e-1 – e-n：glass microfibers for signal transport；f：Optical spectroscopy (e.g. micro optical fiber spectroscopy-S2000, Spectropro-150, surface enhanced Raman spectroscopy; g: the sealed microchannels). (Adapted from reference Y. Song, China Patent, Appl. No. CN200910085973.9)

Song has investigated the efficiency of this kind of biosensing system. Using the color change and LSPR spectra shifts based on the binding of one model biomolecule pairs (anti-body: IgG is firstly functionalized on the Ag surfaces by EDC process, then the antigen: protein-A buffer solution is pumped into the microfluidic channels) as model, it can be seen that the spectra shift and the color changes from the binding of the model biomolecule pairs depend on the concentration of biomolecules and the running time. Up to now, the detection resolution of this kind of biosensors based on the scattering from single Ag NPs has reached 2 nm peak shift per 1 nM concentration change and the resolution for one single NP biosensor is calculated as 10-20 biomolecules per Ag NP(Song 2009). This result suggests another persepctive application by the combination of NSL, microfluidics and bio-functionalization process.

5. Fabrication of hierarchically ordered nanowire arrays on substrates by combination of NSL and Porous anodic alumina (PAA)

In some applications of nanomaterials, the NPs need to be arranged in some particular patterns, architectures or motifs with controlled interspacing, or conjugated with some other kinds of materials (e.g. polymers) (Chong, Zheng et al. 2006; Song , Zhang et al. 2011). The controlled arrangement and immobilization of Ag NPs on substrates will be very crucial to enable some fascinating and delicate applications, particularly in electronic circuit based electro-optical devices and long term functional composites for biological applications. Many methods have been explored for this purpose. Among them, template-assisted LIGA or structure controlled artificial fabrication methods (e.g. E-beam LIGA, NSL, PAA-LIGA) may be the most convenient techniques(Song , Zhang et al. 2011). In the NSL development, the suitability and powerful ability in the architecture and interspacing controlled fabrication of NPs and nanoarrays can be expanded extremely if the NSL can be combined with other template-assisted LIGA methods. Here we just show one example to fabricate hierarchically ordered nanowire arrays on substrates by the combination of NSL and porous anodic alumina (PAA) LIGA(Chong, Zheng et al. 2006).

Like NSL, porous anodic alumina (PAA) templates have attracted intense attention in nanodevice-oriented fabrication in recent years(Xu, Meng et al. 2009). As a well-developed template, PAA offers amazing simplicity and convenience for nanofabrication due to the capabilities of forming high-density, well-aligned, and hexagonally packed sub-100-nm pores, the ability to control the 3D pore structures by simply varying the anodization conditions, and the ease of selectively removing the template after fabrication(Chong, Zheng et al. 2006). As shown in Figure 12, one typical PAA-LIGA process includes(Lombardi, Cavallotti et al. 2007): (a) formation of a 300 nm thick PAA film on Al by a two step anodization process in 0.3M oxalic acid; (b) dissolution of unoxidized Al; (c) barrier layer etching in 5wt% phosphoric acid; (d) transfer of the PAA mask onto Au-coated Si followed by a thermal treatment to improve the adhesion of the films to the substrate; (e) Ag electrodeposition through the PAA pores; (f) PAA mask removal. By carefully controling the sizes and interpore spacing of the nanoholes, very uniform Ag nanorods with controlled interspacing can be fabricated by electroplating. The typical Ag nanorods prepared by this template assisted electrodeposition process can give a much uniform size and interparticle spacing distribution, with a standard size deviation less than 5% and a spacing deviation less than 7%.

Progresses in PAA-LIGA have shown its abilities not only in the synthesis of the traditional high aspect ratio nanomaterials, such as nanorods (Pan, Zeng et al. 2000; Lombardi, Cavallotti et al. 2007; Xu, Meng et al. 2009)and nanowires (Hong, Bae et al. 2001; Xu, Zhang et al. 2005), but also some unique nanostructures, such as porous metallic nanorods by galvanic exchange reaction (Mohl, Kumar et al. 2010), Y-junction nanowires and multiply branched nanomaterials due to its flexibility in the pore structure control according to the principle $1/\sqrt{n} \times V_s$, where V_s is the anodizing voltage for stem pores and n is the number of branched pores from that stem(Meng, Jung et al. 2005; Xu, Meng et al. 2009).

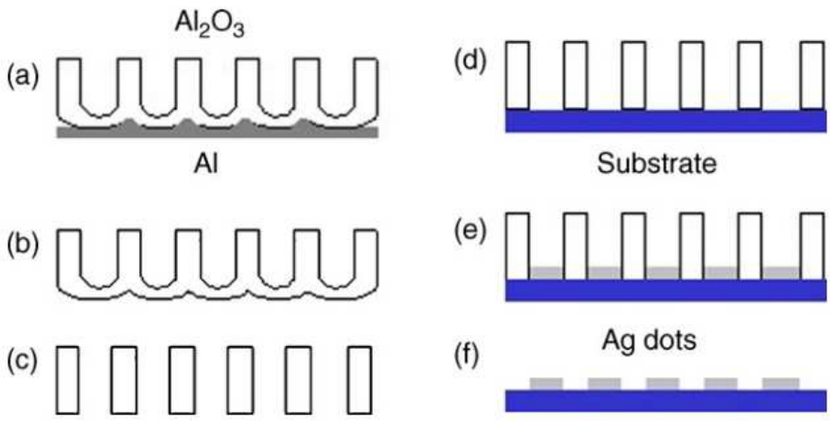

Fig. 12. Fabrication scheme for Ag nanoparticle arrays: (a) formation of a PAA film on Al by a two step anodization process in 0.3Moxalic acid; (b) dissolution of unoxidized Al; (c) barrier layer etching in 5 wt.% phosphoric acid; (d) transfer of the PAA mask onto Au-coated Si followed by a thermal treatment to improve the adhesion of the films to the substrate; (e) Ag electrodeposition through the PAA pores; (f) PAA mask removal. (Lombardi I.; et al., Sensors and Actuators B: chemical 2007, 125, 353-356, Figure 1. Copyright (2007) Elsevier.)

The combination of NSL and PAA-LIGA has been further developed to create hierarchically ordered nanowire arrays, as schematically shown in Figure 13A(Chong, Zheng et al. 2006). A monolayer of self-assembled polystyrene nano or microspheres as masks is first used to deposit periodic porous gold films on silicon substrates (Figure 13A: i-ii). Next, PAA films are fabricated on top of the porous gold film/substrate (Figure 13A: iii). Nanowires are then selectively electrodeposited into the pores of the alumina using the porous gold film as a working electrode (Figure 13A: iv-vi). In detail, a drop of polystyrene sphere suspension (e.g. 1 μm in diameter, 10 wt % aqueous dispersion) is spin-coated onto a pretreated substrate (e.g. Si, glass or mica) to form close-packed microsphere monolayers. The size of the nano or microspheres can be tuned using O_2 reactive ion etching (RIE) with a suitable O_2 flow (e.g. 20 SCCM, SCCM denotes cubic centimeter per minute at STP) at a certain pressure (e.g. 15 mTorr) and a power density (e.g. 110 W) for 6–10 min. After RIE, isolated nano or microsphere monolayers with tunable spacing will be formed. Then, about 5 nm Ti (as an adhesion layer) and 40 nm gold films in turn deposit onto the substrate using the RIE reduced nano or microspheres as masks. After removal of the mask by sonicating in a solvent (e.g. toluene) for 3 min, a porous gold film will be formed on the substrate. After that, an aluminum film with a

thickness of ~500 nm deposits onto the porous gold film. Prior to anodization, the aluminum film is subjected to an imprinting step, in which a free-standing PAA with a thickness of ~10 μm fabricated by the process in Figure 12 is used as a mold for imprinting. Finally, the imprinted aluminum film is anodized in 0.3*M* oxalic acid at 2 °C and the barrier layer at the bottom is removed in 5 wt % H_3PO_4 for 60 min. The gold nanowires can be deposited at −1.0 V versus standard calomel electrode (SCE) from a commercial bath (Orotemp 24, Technic) for varying amounts of time. Alumina templates can be removed in 1M KOH for some time (e.g. 10 min) to obtain hierarchically patterned free-standing nanowires or nanorods.

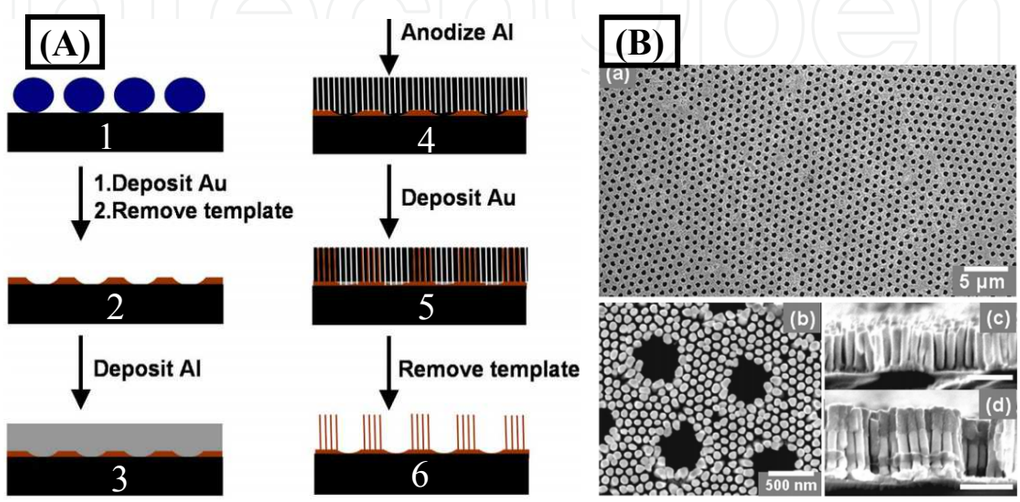

Fig. 13. (A: 1-6) Schematic of method to create hierarchical nanowire arrays on substrates. (B) SEM images of hierarchical nanowire arrays on substrate:(a) Top view of the nanowire arrays with hexagonally organized microvoids over large areas; (b) High magnification SEM image of (a); (c) Side view of the cleaved sample from (a), the concaves caused by voids are clearly apparent; (d) Side view of Au/Ni/Au/Ni segmented nanowire arrays. The side view shows clear contrast; brighter segment is gold portion. Scale bars in (c) and (d): 500 nm. (Chong, M. A. S.; et al., Appl. Phys. Lett. 2006, 89, 233104. Figure 1 and Figure 3. Copyright (2006) from American Institute of Physics. Adapted with permission.)

Figure 13B (a) shows the top view of one typical nanowire arrays with hexagonally organized microvoids (e.g. 500 nm in diameter) over large areas (Chong, Zheng et al. 2006). One of its high magnification images as shown in Figure 13B(b) clearly demonstrates the arranged patterns by individual gold nanowires. The nanowires with uniform size, replicated from the PAA, are hexagonally packed at the nanoscale. The hierarchical nanowire arrays standing on the substrate are further checked from a cleaved sample by side view SEM images (Figure 13B(c), suggesting the well aligned nanowires and the concave features from the nanoscale voids. In addition to fabricating pure gold nanowire arrays, this combinational template is also suitable for selectively electrodepositing other materials for functional device applications. In particular, the vertical structure/composition along the length of the nanowire is also tunable. For example, multilayer Au/Ni/Au/Ni nanowire arrays with in-plane hierarchical structure can be fabricated by the alternating deposition twice of nickel from a Watt's bath (300 g/L $NiSO_4 \cdot 6H_2O$, 45 g/L each H_3BO_3 and $NiCl_2 \cdot 6H_2O$) and of gold at −1.0 V versus SCE electrode. Figure 13B(d) shows the cross section of Au (bottom, brighter segment) /Ni (darker segment)/Au/Ni (top) nanowire arrays.

6. Solution phased nanomaterials by the releasing of nanoparticles fabricated by NSL

Recent progress in nanosphere lithography (NSL) has shown that this method provides a good template for shape-controlled fabrication of surface confined NPs(Zhang, Whitney et al. 2006; Song , Zhang et al. 2011), which also allows for flexible functionalization of these NPs on the clean surface (as cartooned in Figure 14A) using the routine functionalization process from equation 1 to 3. After the surface functionalization of surface confined nanoparticles fabricated by NSL, they can be dislodged into solution phase (as schemed in Figure 14B). This dislodging process provides a useful alternative to synthesis uniform solution phase NPs besides the wet chemical process. Van Duyne *et al.* have developed this process and used it to fabricate solution phase NPs in ethanol(Amanda, Zhao et al. 2005). However, their results indicated that most of the NPs in the solution have nonuniform surface morphologies with truncated tips in addition to the presence of debris and some of the NPs attached together on the glass substrate surface causing the agglomeration of the released NPs. In addition, aqueous phase NPs are expected to be more biocompatible than those in ethanol. Therefore, technology development to obtain aqueous-stable nanocolloids via surface modification and releasing of the surface-confined NPs fabricated by NSL into water solution are much desired.

Our group recently developed a modified NSL process to fabricate Ag NPs with controlled shapes on glass substrates and with the ability to release them into the aqueous solution without any obvious agglomeration(Song and Elsayed-Ali 2010). Three modifications of the standard procedure of nanosphere lithography were made in order to obtain stable NPs with different shapes. The modification to the process were the following: (1) Releasing the nanospheres by immersing the cover slip into a 5% HCl solution for 30 minutes, then immersing the glass substrates into CH_2Cl_2 for 30 s, then sonication for ~20-60 s; (2) The fabricated Ag nanoprisms on the glass substrates were annealed at 100-300 ^oC for 2-5 hours then cleaned by immersing the glass cover slip into 5% HNO_3 for 10-20 s to remove any surface contamination and dissolve debris around the NPs, and then washed by large amount of nanopure water; (3) The glass substrates were immersed into 5-10wt.% HF and HCl acid mixture (HF: HCl = 1:1) for 30-60 s or 10% NaOH solution for 60-120 s to etch part of the glass substrate under the Ag NPs, and then the substrates were washed with sufficient amounts of nanopure water. Finally, the glass substrates with the Ag NPs were dried by inert gas flow and kept in desiccators. The surfaces of the Ag NPs can be modified by chemicals containing thiol groups (such as 1-OT, MUA, 6-MCH and Tiopronin (TP)) forming strong sulfur-silver covalent bonds. We used 1-OT and MUA as functional reagents. The functional solution was prepared by dissolving 0.049 g 1-OT and 0.073 g MUA into 100 mL pure ethanol in a 100 mL volume certificated flask to form 2mM 5:1 1-OT /11-MUA solution. The Ag NPs were once again cleaned using 5 % nitric acid and then immersed into the 2 mM 5:1 1-OT /11-MUA solution and left overnight. The releasing aqueous solution contains 5 V% of 2mM 5:1 1-OT /11-MUA in nanopure water. The glass substrates with surface modified Ag NPs were removed from the functional solution and immersed into the releasing solution. The NPs was then sonicated for 30-120 s to remove them from the substrates into the releasing solution. For a 2-4 mL releasing solution, 4-8 glass substrates were used in order to reach a NP concentration suitable for optical property measurements.

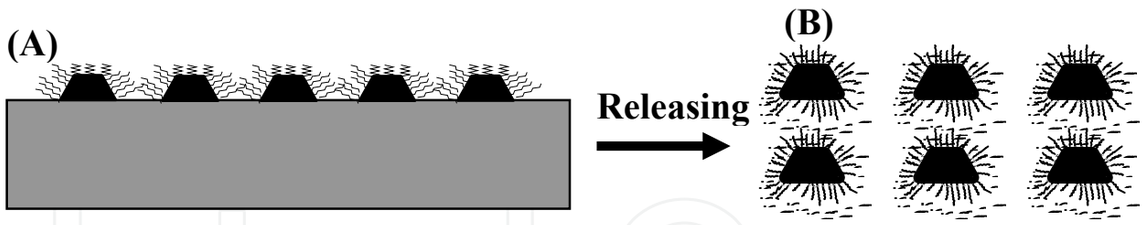

Fig. 14. (A) the surface-confined triangular Ag NPs are functionalized by chemicals with thiol groups and (B) can be further released into water or other solvents forming solution-phased nanocolloids. (Adapted from reference Y. Song, China Patent, Appl. No. CN200910085973.9)

Comparing with those Ag NPs via the traditional dislodging method(Amanda, Zhao et al. 2005; Song and Elsayed-Ali 2010), the shape integrity of the heat-treated NPs after releasing them into water can be retained perfectly. Figure 15(a) shows TEM image of the Ag NPs after thermal annealing without pre-sonication. Most of those Ag NPs show triangular shapes with rounded tips (doted circles in Fig. 15(a)) and some with snipped tips (dashed circles in Fig. 15(a)). The inset is a magnified image of these NPs, clearly showing a triangular shape with rounded tips. The histogram for these Ag NPs (Fig. 15(b)) gives a mean size of 39.6 ± 4.9 nm with much narrower size distribution of STDEV % = 12.4 % than those obtained from surface-confined Ag NPs without any post annealing (STDEV % = 41.7 %)(Song and Elsayed-Ali 2010). Fig. 15(c) is a TEM image for Ag NPs that were thermally annealed after removing two tips by sonication, whose histogram gives a mean size of about 33.9 ± 6.8 nm (Fig. 15(d)), less than that for those triangular shaped NPs with rounded tips after post-annealing. Most of these NPs show quadrilateral shapes (dashed circles) or pentagon shapes as shown more clearly in the inset of Fig. 15(c). These NPs have a similar shape as those observed by AFM images in Figs. 6(c-1) and (c-2). From the TEM images in Fig. 15(c), some of the NPs give less contrast in their central parts (NPs labeled by dashed circles). We believe that the lighter centers in these NPs are from a thinner center resulting from adhesion of the center of these NPs to the glass substrate during annealing. AFM observation of the glass substrate after removal of the NPs show debris forming hexagonal shaped arrangements. This observation is consistent with adhesion of the central part of the triangular nanoprisms to the substrate.

Variations in the shape, surface modification and surrounding environment of these NPs give significant shifts in their UV-vis absorption spectra for the surface confined NPs before and after tip rounding, after surface modification, and after dislodging into water, as shown in Figure 16. The absorption spectrum for the surface-confined Ag NPs fabricated by NSL without any tip rounding and surface modification has two distinct peaks at 476 nm and 672 nm (Figure 16a). The absorption peak at 476 nm is primarily from the higher-order mode surface plasmon resonance (e.g., quadrupole) of the NPs, and the peak at 672 nm is mainly from the dipole resonance of the NPs. We note that the higher-order resonance peak has almost the same intensity as that for the dipole resonance for all types of NPs, although the higher order modes are expected to be much weaker than the dipole resonance. Since the substrate is continuously covered by a hexagonally arranged array of Ag NPs with tip-tip distance less than 100 nm, we postulate that the particle-particle coupling will contribute to the LSPR spectrum. This particle-particle interaction effect could be responsible for the observed spectrum. When the tips in the Ag triangular nanoprisms are rounded, the tip-tip

LSPR coupling effects are alleviated, as indicated by the disappearance of the peak at 672 and the red-shift of the peak at 476 nm to 504 nm representing the higher-order surface plasmon resonance mode (Figure 16b). The absorption spectrum for the surface modified Ag NPs (Fig. 16c) shows a slight blue shift at the peak of 476 nm (to 470 nm) and a significant blue shift at 672 nm (to 626 nm) with reduced intensities. This spectrum was expected to give a red shift due to the increased dielectric constant from the adsorbed thiol compounds(Amanda, Zhao et al. 2005). We attribute this blue shift to shape variation (e.g., increased height, smooth surface topography) during surface modification by immersion that was similar to solvent annealing which results in blue-shift of LSPR since any solvent annealing has not been done on our NPs(Jensen, Duval Malinsky et al. 2000; Malinsky, Kelly et al. 2001). These variations have been observed by the slightly reduced NP size and rounded shapes observed in the TEM image of Figure 15 when compared with the AFM image of Figure 1 and Figure 6. In addition, when the Ag NPs are covered by thiol groups, the surface free electron density may be reduced, leading to weaker surface plasmon resonance in single NPs and surface plasmon resonance coupling among nanoparticle arrays(Kelly, Coronado et al. 2003). This will result in a blue shift of the LSPR peak and a reduced LSPR intensity.

The UV-vis absorption spectrum of the Ag NPs after release in water, shown in Fig. 16d, was compared to other surface confined NPs. The aqueous Ag NPs give a main peak at 532 nm and a very weak peak at 352 nm. The main peak at 532 nm appears to be from LSPR by the triangular nanoprisms with rounded tips and is blue shifted from that obtained for NPs with a LSPR peak at 605 nm fabricated by the routine NSL and released from the surface. This is attributed to the reduced size and rounded tips. The peak at 352 nm in Fig. 16d becomes much weaker and narrower than that for the aqueous Ag NPs released from the surface confined Ag NPs as fabricated by routine NSL, obviously due to the shape variation of NPs and almost no small spherical shaped debris observed in the aqueous Ag NPs released from the surface-confined Ag NPs fabricated by the modified NSL (Figure 16a). By comparing the TEM images for the two kinds of Ag NPs, it can be deduced that the peak at 352 nm in Fig. 16d is mainly from the out-of-plane quadrupole resonance of Ag nanoprisms with rounded tips according to the previous investigation(Jin, Cao et al. 2001; Amanda, Zhao et al. 2005; Zhang, Li et al. 2005). The peak intensity ratio between the main peak at 532 nm and the weak peak at 352 nm for these NPs is ~11.5:1 (after subtracting the background), which is much higher than that for the NPs obtained by the routine NSL and releasing process (1:3.6)(Song and Elsayed-Ali 2010). Clearly, the number of the small debris caused by the sonication is greatly reduced using the modified NSL and releasing process. The modified NSL process favors the formation of uniform Ag NPs with rounded tips with significant reduction in Ag debris, as shown in Fig. 15. In addition, 1-OT and 11-MUA can be substituted by the combination of 1-BT and TP, or MCH and MUA if more water-soluble NPs are desired.

Clearly, Ag NPs with controlled shapes and reduced defect density can be fabricated by a modified NSL process. Upon dislodging these NPs into a solution, they retain their shapes significantly better than NPs produced by routine NSL. Thus, aqueous phase Ag NPs with relatively uniform size and shape distribution can be fabricated. The UV-vis absorption spectra for surface confined NPs show two distinct absorption peaks (Figure 16a), comparing with those with rounded tips (Figure 16b). After surface modification, the central wavelengths of the two absorption peaks blue shifted and showed reduced intensities. The

aqueous phased Ag NPs produced by the modified NSL method show a main peak and another peak with very low intensity attributed mainly to small debris produced during the dislodging process. The noticeable reduction in the intensity of the short wavelength peak for the modified NSL method compared to the routine method is due to the significant reduction in Ag debris. TEM images show that the uniformity of Ag NPs can be improved significantly by the modified NSL and releasing processes.

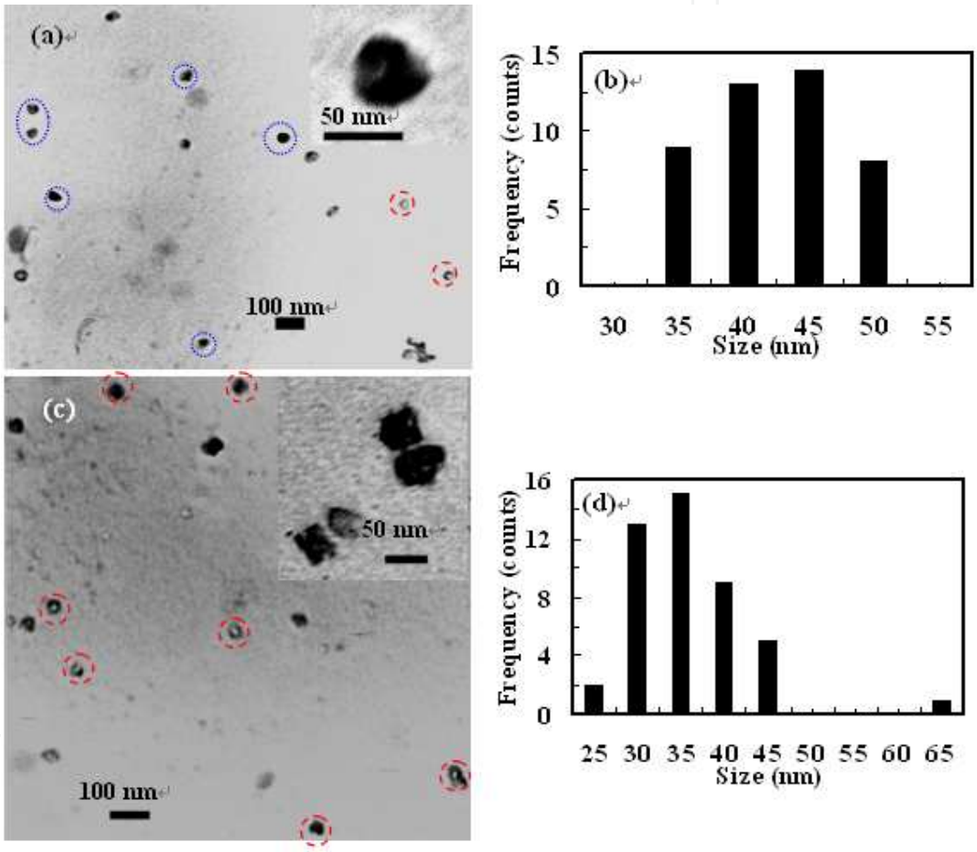

Fig. 15. TEM images of the aqueous phase Ag NPs after surface modification by thiol compounds and dislodging from the glass substrate. (a) Triangle Ag NPs with rounded tips. Dashed circles: Ag NPs with rounded tips; dotted circle: Ag NPs with slightly rounded tips. (b) Histogram of triangular shaped Ag NPs with rounded tips based on 45 NPs giving a mean size of 39.6±4.9 nm. (c) Quadrilateral and pentagon shaped Ag NPs. Dashed circles: some typical Ag NPs with quadrilateral shapes. (d) Histogram of quadrilateral and pentagon shaped Ag NPs based on 45 NPs giving a mean size of 33.9±6.8 nm. (Reprinted from Song et al., Appl. Surf. Sci. 2010 256, (20), 5961, Figure 4. Copyright (2010) Elsevier.)

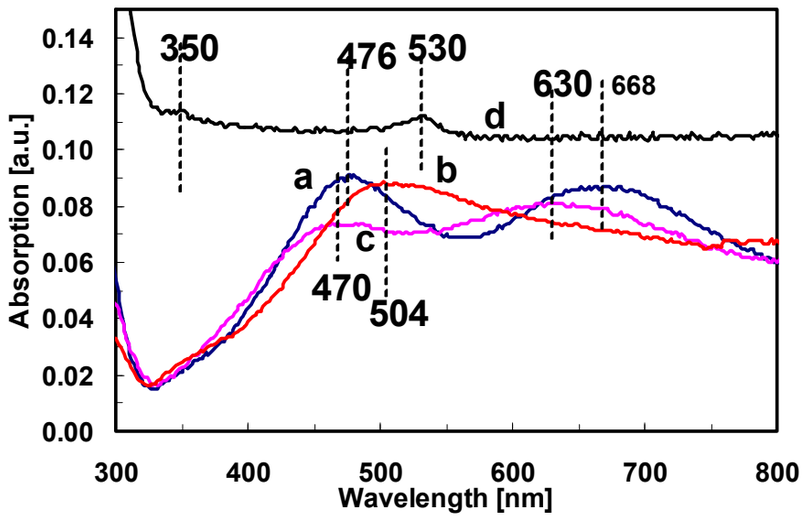

Fig. 16. UV-vis optical absorption of Ag NPs. (a) Surface confined Ag NPs before tip rounding and surface modification. (b) Surface confined Ag NPs after tip rounding (c) Surface confined Ag NPs with rounded tips after surface modification with thiol. (d) Aqueous phase Ag NPs after releasing the surface confined NPs into water. (Adapted from Song et al., Appl. Surf. Sci. 2010 256, (20), 5961, Figure 5. Copyright (2010) Elsevier.)

7. Perspective for the NSL in the controlled fabrication of nanomaterials

The great progress in controlled synthesis/fabrication of noble metal NPs by NSL, and the increase in the experimental and theoretical achievements in control of their size, shape, surface morphology and 3-dimensional space orientation dependent physicochemical properties and functions suggest expanding application in many fields because of the potential for essential breakthroughs by researchers and engineers for more advanced applications of NSL. Particularly, the developed multi-step angle resolved NSL and the modified NSL incorporated with suitable post-treatments have enabled us to obtain uniform surface-confined overlapped and nano-gapped nanostructures, the tip-rounded triangular nanoprisms, the square-shaped and the trapezoidal nanoprisms, besides the common triangular nanoprisms. Besides the marvelous progresses in the surface-confined nanostructures fabrication, a modified NSL process has also been developed to dislodge these uniform nanomaterials into the desired solvents (e.g. water, ethanol) without any obvious agglomeration as in the solution-phased nanocolloids synthesis.

Progresses in the incorporation of NSL with other LIGA techniques have shown that the suitability and ability in the architecture and interspacing controlled fabrication of NPs and nanoarrays. Their applications can thus be expanded extremely. When the multi-hierarchy arrayed micro windows fabricated by the traditional UV-LIGA process is joined in NSL, one powerful method for single nanoparticle identification will be born, resulting in the possibility of the precise investigation of the 3D morphology dependent LSPR of nanoparticles and LSPR coupling in nanoarrays. By collaboration with UV-LIGA microfabrication, uniform noble metal nanoparticles or nanoarrays can be fabricated into the targeted micro channels, leading to a much sensitive optical biosensing system after their

surfaces are modified by the traditional functionalization process. By combination of PAA-LIGA and NSL, the possibility for building hierarchically ordered multi-segment nanowires or nanorods will be realized conveniently.

Summarizing from the recent progresses and discussion on NSL presented in this chapter, four main researches thrust that includes several active and challenging topics may form the primary research focuses and directions in this particular field. One is the fabrication technique development for the formation of monolayer of nanospheres with uniform area as large as several centimeter squares, which founds the basis of NSL. Another is the convenient and practical process in the releasing of these surface confined nanomaterials into solvent with perfectly retained 3D morphologies, which is still challenging but a desired alternative to obtain the uniform nanomateirals besides the well-developed wet chemical process. The third is the advanced incorporation of NSL with other fabrication techniques besides LIGA processes for the building more complex 3D hierarchically ordered nanostructures, which will definitely make a breakthrough in the nanoscale device and assemble development. The fourth may be the fabrication of tunable hetero-structure-composition nanocomposites, such as sandwich discs or multi-layer nanostructures, which will produce hetero-nanostructures with multi-functions (e.g. magntic, optical, electronic, etc). Consequently, outcomes of these challenging researches will result in the discovery of many exciting and versatile techniques for nanomaterials fabrication, and theoretical breakthrough in their novel physicochemical properties and for advanced applications.

8. Acknowledgement

The author appreciates the support fromthe Fundamental Research Funds for the Central Universities (Vision Funds of Beihang University: YWF-11-03-Q-002) and NSFC (Grant No. 50971010)

9. References

Ahmadi, T. S.; Wang, Z. L.; et al. (1996). "Shape-Controlled Synthesis of Colloidal Platinum Nanoparticles." Science 272: 1924-1927.

Amanda, H. J.; Zhao, J.; et al. (2005). "Solution-Phase, Triangular Ag Nanotriangles Fabricated by Nanosphere Lithography." J. Phys. Chem. B 109(22): 11158-62.

Brayner, R. (2008). "The toxiccological impact of nanoparticles." Nano Today 3(1-2): 48-55.

Chong, M. A. S.; Zheng,Y. B.; et al. (2006). "Combinational template-assisted fabrication of hierarchically ordered nanowires arrays on substrates for device applications." Appl. Phys. Lett. 89: 233104-1-3.

Daniel, M.-C. and Astruc, D. (2004). "Gold Nanoparticles: Assembly, Supramolecular Chemistry, Quantum-Size-Related Properties, and Applications toward Biology, Catalysis, and Nanotechnology." Chem. Rev. 104: 293-346.

Dhar, P.; Cao, Y.; et al. (2007). "Autonomously Moving Local Nanoprobes in Heterogeneous Magnetic Fields." J. Phys. Chem. C 111: 3607-3613.

Edwards, H. W. and Petersen, R. P. (1936). "Reflectivity of evaporated silver films." Phys. Rev. 9: 871.

Erhardt, D. (2003). Materials conservation: Not-so-new technology Nature Materials 2: 509-510.

Haes, A. J.; Zou, S.; et al. (2004). "A Nanoscale Optical Biosensor: The Long Range Distance Dependence of the Localized Surface Plasmon Resonance of Noble Metal Nanoparticles." J. Phys. Chem. B 108: 109-116.

Hammond, C. R. (2000). The Elements, in Handbook of Chemistry and Physics 81th edition, CRC press.

Haynes, C. L.; Mcfarland, A. D.; et al. (2003). "Nanoparticle Optics: the Importance of Radiative Dipole Coupling in Two-Dimensional Nanoaprticle Arrays." J. Phys. Chem. B 107: 7337-7342.

Haynes, C. L. and van Duyne, R. P. (2001). "Nanosphere Lithography: A Versatile Nanfabrication Tool for Size Dependent Nanoparticle Optics." J. Phys. Chem. B 105: 5599.

Hong, B. H.; Bae, S. C. et al. (2001). "Ultrathin single-crystalline silver nanowire arrays formed in an ambient solution phase." Science 294: 348-351.

http://en.wikipedia.org/wiki/Silver.

Hulteen, J. C.; Treichel,D. A.; et al. (1999). "Nanosphere Lithography: Size-tunable silver nanosparticle and surface cluster arrays." J. Phys. Chem. B 103: 3854-3863.

Jain, P. K.; Huang, X.; et al. (2007). "Review of some interesting surface plasmon resonance-enhanced properties of noble metals nanoparticles and their applicaitons to biosystems." Plasmonics 2: 107-118.

Jensen, T. R.; Duval Malinsky, M.; et al. (2000). "Nanosphere Lithography: tunable localized surface plasmon resonance spectra of silver nanoparticles." J. Phys. Chem. B 104: 10549-10556.

Jin, R.; Cao,Y. W.; et al. (2001). "Photoinduced conversion of silver nanospheres to nanoprisms." Science 294: 1901-1904.

Kelly, K. L.; Coronado, E.; et al. (2003). "The optical proeprties of metal nanoparticles: the influence of size, shape and dielectric environment." J. Phys. Chem. B 107(3): 668-677.

Kreibig, U. and Vollmer, M. (1995). Optical Properties of Metal Clusters. Berlin, Springer.

Lee, S. J.; Morrill, A. R.; et al. (2006). "Hot spots in silver nanowire bundles for surface-enhanced Raman spectroscopy." J. Am. Chem. Soc. 128: 2200-2201.

Lombardi, I.; Cavallotti, P. L.; et al. (2007). "Template assisted deposition of Agnanoparticle arrays for surface-enhanced Raman scattering applications." Sensors and Actuators B: Chemical 125: 353-356.

Malinsky, M. D.; Kelly, K. L.; et al. (2001). "Chain length Dependence and sensing capabilities of the localized surface plasmon resonance of silver nanoparticles chemically modified with alkanethiol self-assembled monolayers." J. Am. Chem. Soc. 123: 1471-1482.

Maneerung, T.; Tokura, S.; et al. (2008). "Impregnation of silver nanoparticles into bacterial cellulose for antimicrobial wound dressing." Carbohydrate Polymers 72: 43-51.

Meng, G.; Jung,Y. J.; et al. (2005). "Controlled fabrication of hierarchically branched nanopores, nanotubes and nanowires." PNAS 102(20): 7074-7078.

Mock, J. J.; Barbic, M.; et al. (2002). "Shape effects in plasmon resonance of individual colloidal silver nanoparticles." J. Chem. Phys. 116(15): 6755-6759.

Mohl, M.; Kumar, A.; et al. (2010). "Synthesis of catalytic porous metallic nanorods by galvanic exchange reaction." J. Phys. Chem. C 114: 389-393.

Noguez, C. (2007). "Surface Plasmons on Metal Nanoparticles: the Influence of Shape and Physical Environment." J. Phys. Chem. C 111(10): 3806-3819.

Ozbay, E. (2006). "Plasmonics:Merging Photonics and Electronics at Nanoscale Dimensions." Science 311: 189-193.

Pan, S. L.; Zeng, D. D.; et al. (2000). "Preparation of ordered array of nanoscopic gold rods by template method and its optical properties." Appl. Phys. A 70: 637-640.

Percival, S. L.; Bowler, P. G.; et al. (2005). "Bacterial resistance to silver in wound care." Journal of Hospital Infection 60: 1-7.

Prasad, P. N. (2004). Nanophotonics. Hoboken, New Jersey, John Wiley & Sons, Inc.

Schwartzberg, A. M. and Zhang J. Z. (2008). "Novel Optical Properties and Energing Applications of Metal Nanostructures." J. Phy. Chem. C 112(28): 10324-10337.

Shen, Y.; Friend, C. S.; et al. (2000). "Nanophotonics: Interaction, Materials and application." J. Phys. Chem. B 104: 7577-7587.

Song, Y. (2009). Fabrication of high throughput biosensors based on single Nanoparticles and Nanoparticle arrays, China Patent, Appl. No. CN 200910085973.9.

Song, Y. (2010). "Fabrication of Multi-level 3-Dimension Microstructures by Phase Inversion Process." Nano-Micro Letters 2(2): 95-100.

Song, Y. and Elsayed-Ali, H. E. (2010). "Aqueous Phase Ag Nanoparticles with Controlled Shapes Fabricated by a Modified Nanosphere Lithography and their Optical Properties." Appl. Surf. Sci. 256(20): 5961-5967.

Song , Y.; Henry, L. L.; et al. (2009). "Stable Cobalt Amorphous Nanoparticles Formed by an In-situ Rapid Cooling Microfluidic Process " Langmuir 25 (17): 10209-10217.

Song , Y.; Jin, P.; et al. (2010). "Microfluidic Synthesis of Fe Nanoparticles." Mater. Lett. 64: 1789-1792.

Song, Y.; Sun, S.; et al. (2010). "Synthesis of Worm and Chain-like Nanoparticles by a Microfluidic Reactor Process." J. Nanopart. Res. 12: 2689-2697.

Song , Y.; Zhang, Z.; et al. (2011). "Identification of Single Nanoparticles." Nanoscale 3: 31-44.

Su, K.-H.; Wei, Q.-H.; et al. (2003). "Interparticle Coupling Effects on Plasmon Resonances of Nanogold Particles." Nano lett. 3(8): 1087-1090.

Vo-Dinh, T.; Wang, H.-N.; et al. (2009). "Plasmonic nanoprobes for SERS biosensing and bioimaging." J. Biophoton.: 1-14.

Xu, C.-l.; Zhang, L.; et al. (2005). "Well-dispersed gold nanowire suspension for assembly applicaiton." Appl. Surf. Sci. 252: 1182-1186.

Xu, Q., Meng, G.; et al. (2009). "A Generic Approach to Desired Metallic Nanowires Inside Native Porous Alumina Template via Redox Reaction." Chem. Mater. 21: 2397-2402.

Yang, Y.; Matsubara, S.; et al. (2007). "Solvothermal synthesis of multiple shapes of silver nanoparticles and their SERS properties." J. Phys. Chem. C 111: 9095-9104.

Zhang, J.; Li, X. et al. (2005). "Surface enhanced raman scattering effects of silver colloids with different shapes." J. Phys. Chem. B 109: 12544-12548.

Zhang, X.; Whitney, A. V.; et al. (2006). "Advances in Contemporary Nanosphere Lithographic Techniques." J. Nanosci. Nanotech. 6: 1920-1934.

Zhao, L. L.; Kelly, K. L.; et al. (2003). "The extinction spectra of Ag nanoparticle arrays: influence of array structure on plasmon resonance wavelength and widths." J. Phys. Chem. B 107: 7343-7350.

Zhou, Q.; Qian, G.; et al. (2008). "Two-dimentional assembly of silver nanoparticles for catalytic reduction of 4-nitroaniline." Thin Solid Films 516: 953-956.

Zhu, S.; Li, F.; et al. (2008). "A localized surface plasmon resonance nanosensor based on rhombic Ag nanoparticle array." Sensors and Actuators B: Chemical 134: 193-198.

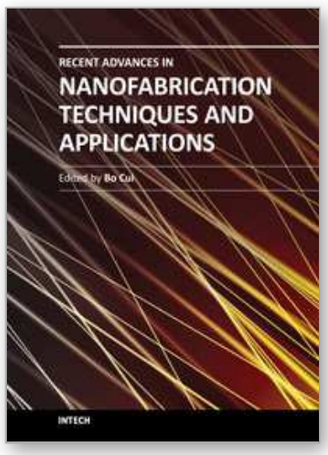

Recent Advances in Nanofabrication Techniques and Applications

Edited by Prof. Bo Cui

ISBN 978-953-307-602-7
Hard cover, 614 pages
Publisher InTech
Published online 02, December, 2011
Published in print edition December, 2011

Nanotechnology has experienced a rapid growth in the past decade, largely owing to the rapid advances in nanofabrication techniques employed to fabricate nano-devices. Nanofabrication can be divided into two categories: "bottom up" approach using chemical synthesis or self assembly, and "top down" approach using nanolithography, thin film deposition and etching techniques. Both topics are covered, though with a focus on the second category. This book contains twenty nine chapters and aims to provide the fundamentals and recent advances of nanofabrication techniques, as well as its device applications. Most chapters focus on in-depth studies of a particular research field, and are thus targeted for researchers, though some chapters focus on the basics of lithographic techniques accessible for upper year undergraduate students. Divided into five parts, this book covers electron beam, focused ion beam, nanoimprint, deep and extreme UV, X-ray, scanning probe, interference, two-photon, and nanosphere lithography.

How to reference

In order to correctly reference this scholarly work, feel free to copy and paste the following:

Yujun Song (2011). Controlled Fabrication of Noble Metal Nanomaterials via Nanosphere Lithography and Their Optical Properties, Recent Advances in Nanofabrication Techniques and Applications, Prof. Bo Cui (Ed.), ISBN: 978-953-307-602-7, InTech, Available from: http://www.intechopen.com/books/recent-advances-in-nanofabrication-techniques-and-applications/controlled-fabrication-of-noble-metal-nanomaterials-via-nanosphere-lithography-and-their-optical-pro

INTECH
open science | open minds

InTech Europe
University Campus STeP Ri
Slavka Krautzeka 83/A
51000 Rijeka, Croatia
Phone: +385 (51) 770 447
Fax: +385 (51) 686 166
www.intechopen.com

InTech China
Unit 405, Office Block, Hotel Equatorial Shanghai
No.65, Yan An Road (West), Shanghai, 200040, China
中国上海市延安西路65号上海国际贵都大饭店办公楼405单元
Phone: +86-21-62489820
Fax: +86-21-62489821

IntechOpen